CHEMISTRY OF MATERIALS

NOVEMBER 12, 2019 | VOLUME 31 | NUMBER 21 | pubs.acs.org/cm

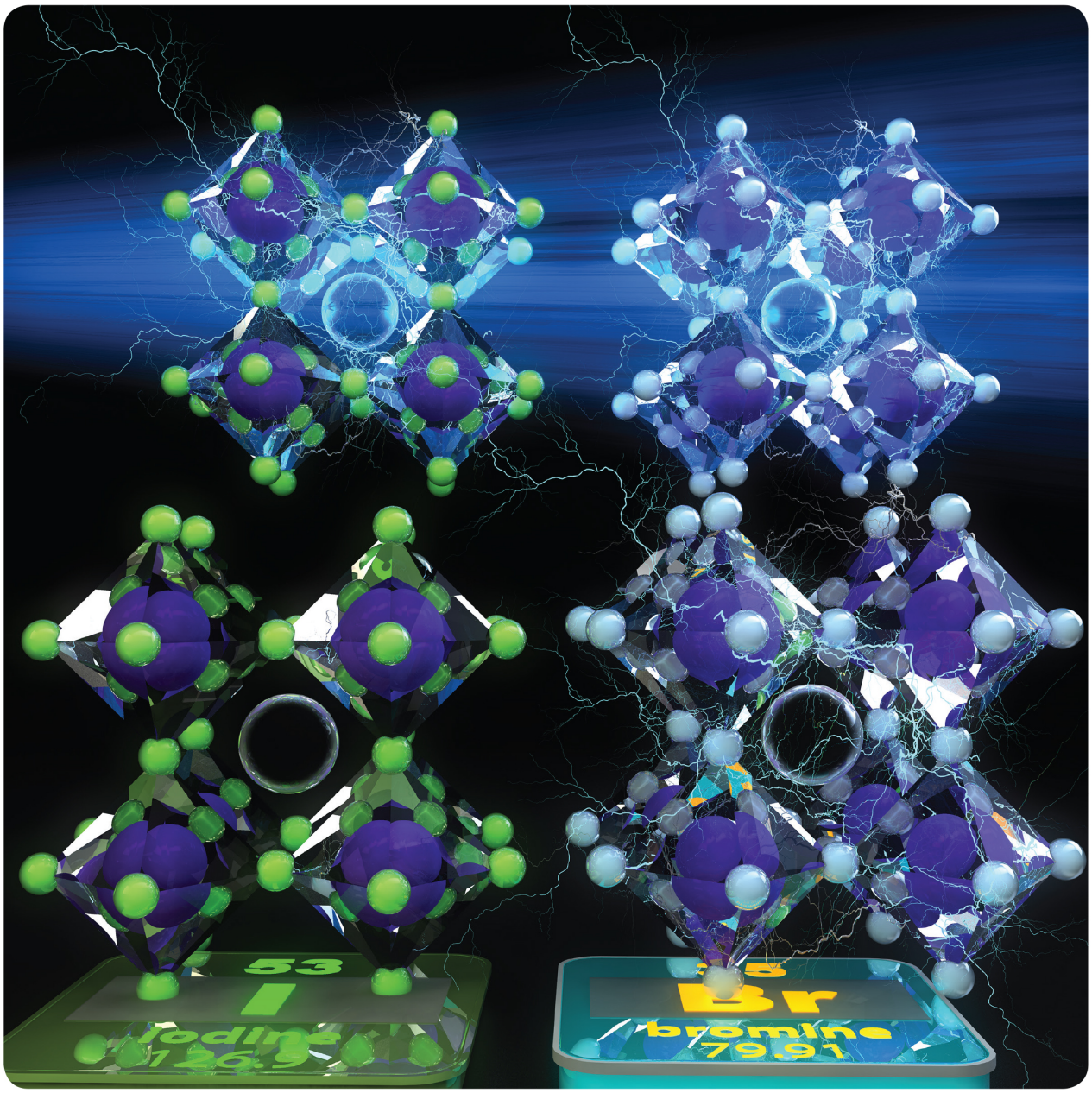

ACS Publications
Most Trusted. Most Cited. Most Read.

www.acs.org

CHEMISTRY OF MATERIALS
Cite This: Chem. Mater. 2019, 31, 8969−8976
Article
pubs.acs.org/cm

The Effects of Incident Photon Energy on the Time-Dependent Voltage Response of Lead Halide Perovskites

Elizabeth M. Tennyson,[†,‡,▽] John M. Howard,[†,‡,▽] Bart Roose,[§] Joseph L. Garrett,[‡,∥] Jeremy N. Munday,[‡,⊥] Antonio Abate,[#,¶] and Marina S. Leite*[,†,‡]

[†]Department of Materials Science and Engineering, University of Maryland, College Park, Maryland 20742, United States
[‡]Institute for Research in Electronics and Applied Physics, University of Maryland, College Park, Maryland 20742, United States
[§]Cavendish Laboratory, Department of Physics, University of Cambridge, JJ Thomson Avenue, CB3 0HE Cambridge, United Kingdom
[∥]Department of Physics, University of Maryland, College Park, Maryland 20742, United States
[⊥]Department of Electrical and Computer Engineering, University of Maryland, College Park, Maryland 20742, United States
[#]Helmholtz-Zentrum Berlin für Materialien und Energie, Kekuléstraße 5, 12489 Berlin, Germany
[¶]Department of Chemical, Materials and Production Engineering, University of Naples Federico II, Piazzale Tecchio 80, 80125 Fuorigrotta, Naples, Italy

Supporting Information

ABSTRACT: Tuning the halide composition in semiconductor perovskite materials is relevant for light-emitting and absorbing applications, as it significantly affects the dynamics of both the optical and electrical properties. Yet, a precise understanding of how the halide species influence the electrical behavior of the perovskite remains vague and speculative. In this work, we elucidate the transient voltage of two pure-halide perovskite film compositions ($CH_3NH_3PbBr_3$ and $CH_3NH_3PbI_3$) to directly compare the role of the halide in ionic species migration. We capture the photovoltage rise and residual voltage relaxation upon switching the illumination ON and subsequently OFF using Kelvin-probe force microscopy. We discover a unique and unforeseen wavelength-dependent voltage decay for $CH_3NH_3PbBr_3$. Here, high-energy photons induce a more than 1 order of magnitude slower voltage decline toward equilibrium (i.e., dark conditions) than low-energy photons. Conversely, we find that the $CH_3NH_3PbI_3$ perovskite composition has a wavelength-independent decay rate. The difference in electrical response occurs primarily because of the halide composition, as ion migration rates are reduced with higher Br content. The results detailed here yield new experimental insights about ion/defect activation energies in different perovskite films and devices, underlining a new parameter, photon energy (wavelength), which must be considered when assessing the fundamental photophysics within these materials.

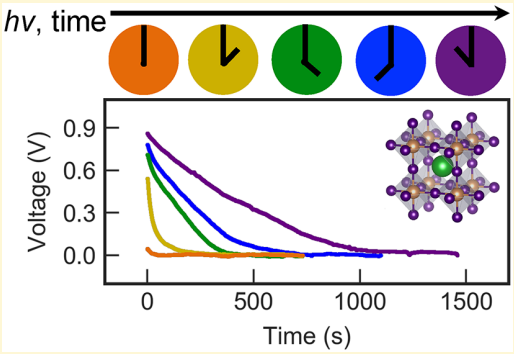

INTRODUCTION

Perovskite solar cells have undeniably yielded fruitful research advances in the photovoltaic (PV) community, despite the shortage of stable devices.[1] Currently, the record power conversion efficiency (η) surpasses 25% due to enhanced material quality via composition engineering, improved charge carrier transport interfaces, and maturing fabrication techniques.[2−6] Perovskite's light absorption properties and electrical output are intimately linked to its chemical composition. For example, in the perovskite ABX_3 structure, where A = Cs^+, $CH_3NH_3^+$ (MA), and/or $HC(NH_2)_2^+$ (FA), B = Pb^{2+}, and X = I^-, Br^-, and/or Cl^-, substituting Br^- for I^- influences charge recombination activity, light-induced halide gradient distributions, and dramatically increases the band gap.[7−9] Despite these exciting developments, perovskites are still incapable of maintaining the stable long-term electrical output required for large-scale deployment. Performance dynamics arise from a variety of external environmental stressors,[1,10] including light,[11] humidity,[12,13] oxygen,[14,15] temperature,[16,17] and bias.[18,19] Incorporating different halides or cations into the ABX_3 lattice can inhibit the effects of some of these extrinsic parameters. Regardless, the most stable perovskite solar cell to date has only provided consistent power output for a year.[20] Thus, while it is recognized what causes a reduction in power conversion efficiency, PV researchers do not yet have a

Received: August 1, 2019
Revised: August 30, 2019
Published: September 4, 2019

DOI: 10.1021/acs.chemmater.9b03089
Chem. Mater. 2019, 31, 8969−8976

complete explanation for *how* the perovskite material deteriorates.

When perovskites endure long periods of sunlight exposure, their performance degrades,[9] and as recently shown, visible light can influence their electrical and optical properties in an unpredicted wavelength (λ)-dependent manner.[21,22] Macroscopic $J-V$ curves under blue and red illumination of a $(FA_{0.67}MA_{0.33})Pb(I_{0.83}Br_{0.17})_3$ perovskite revealed that shorter λ photons (bluer) cause more hysteresis than red light.[21] This phenomenon is described by thermal-assisted ion movement or vacancy generation, as higher-energy photons yield more abundant and/or energetic phonons. Further, λ-dependent photoluminescence (PL) measurements of $CH_3NH_3PbI_3$ show that illuminating the perovskite with <520 nm light causes PL degradation, while photon excitation >520 nm induced photo brightening.[22] These optical processes are explained by the presence of excess PbI_2 (band gap = 2.38 eV, ~ 520 nm) and its participation in photolysis reactions that degrade the perovskite absorber.[23] Moreover, recent density functional theory (DFT) calculations suggest that the halide atom in the perovskite could be the primary source of the unique photoexcitation reliance, as the replacement of I^- with Br^- causes the crystal lattice to compress, ultimately reducing ion migration.[24] This decrease in motion with increased Br^- content is also confirmed through calculations of activation energies (E_A), where Br^- defects require extra energy to move[25] than I^- defects. Thus, bluer light facilitates mobile vacancies and interstitials more than red.

To understand the impact of ion motion on perovskites' electrical response, it is essential to utilize an experimental approach that acquires data at relevant time scales. Heterodyne Kelvin probe force microscopy (KPFM) directly measures the open-circuit voltage (V_{oc}) in real time,[26−28] with a temporal resolution of ~1 ms, which is suitable for accurate extraction of ion migration rates within perovskite solar cells.[29] Other implementations of KPFM have shown a time resolution down to 10−100 μs, revealing charge carrier accumulation at the perovskite−electrode interface; however, in this case, the electrical data extraction occurs postacquisition.[30] Transient-absorption (TA) microscopy probes the charge-carrier transport behavior and visualizes electron and hole movement across perovskite grain boundaries[31] with a ps to ns time resolution, which is too fast to capture ionic motion.[32,33] PL measurements have had excellent success at tracking the shift in the local bandgap due to halide segregation on the time range of seconds.[34] Yet, PL's information is limited to probing perovskite's optical properties, yielding little quantitative information about the electronic and ionic transiency. Therefore, in order to capture the voltage dynamics associated with ion migration in perovskites, we implement illuminated heterodyne KPFM.[35,36]

Here we identify the wavelength-dependent electrical properties of two pure-halide perovskite compositions ($CH_3NH_3PbBr_3$ and $CH_3NH_3PbI_3$) by monitoring the voltage response across single-wavelength illumination cycles. We discover a slow, λ-dependent, voltage relaxation, ranging from 26 s up to 14 min, for the $CH_3NH_3PbBr_3$ material, whereas the archetypal $CH_3NH_3PbI_3$ sample's residual voltage relaxation time is entirely unaffected by the incident photon energy. Interestingly, upon initial illumination, the voltage dynamics are almost as fast as the data acquisition rate and there is no correlation with wavelength, indicating that electronic charge carriers dominate the initial photovoltage response. We reveal that with enough time in the dark (≈1000 s), the electrical response equilibrates back to its initial value, demonstrating the exceptional recoverability of the perovskite solar cell materials considered here. Throughout, the energy of incident photons correlates with the rate and amount of ionic movement. However, the $CH_3NH_3PbBr_3$ lattice constrains the diffusion of all ionic species back to their equilibrium positions, while the comparatively open lattice of $CH_3NH_3PbI_3$ allows for a more rapid voltage relaxation response. Our findings highlight a relatively unexplored parameter to probe perovskite dynamics, photon energy, and establish the ability to control ion migration time scales by tuning the illumination source.

EXPERIMENTAL METHODS

Halide Perovskite Fabrication. All chemicals are from Sigma-Aldrich, unless stated otherwise. Fluorine-doped tin oxide coated glass slides (Solaronix, 8 Ω/□) were cleaned and sonicated in 2% Hellmanex solution for 15 min, rinsed with deionized water, sonicated in acetone for 15 min, rinsed with acetone, sonicated in isopropanol for 15 min, and finally rinsed with isopropanol and dried with air. The substrates were then subjected to an O_2 plasma treatment immediately before the deposition of the 30 nm TiO_2 electron selective layer. The TiO_2 was deposited by spray pyrolysis at 450 °C from a precursor solution of titanium diisopropoxide bis-(acetylacetonate) (0.6 mL, 75 wt % in isopropanol), acetylacetone (0.4 mL) in anhydrous ethanol (9 mL). The substrates were left to cool to room temperature. Subsequently, a 150 nm thick mesoporous TiO_2 layer was deposited by spin coating a 30 nm particle paste (Dyesol 30 NR-D) diluted in ethanol (150 mg/mL) for 10 s at 4000 rpm with a 2000 rpm ramp rate. After they were spin coated, the substrates were dried at 150 °C for 10 min and sintered at 450 °C for 30 min. The substrates were cooled to 150 °C and immediately transferred to a nitrogen-filled glovebox.

$MAPbI_3$ was deposited from a solution containing PbI_2 (1.2M, TCI) and MAI (1.2M, Greatcell Solar) in anhydrous DMSO, and $MAPbBr_3$ from a solution containing $PbBr_2$ (1.3M, TCI) and MABr (1.2M, Greatcell Solar) in anhydrous DMF:DMSO 4:1 (v/v). Perovskite solutions were spin coated using a two-step protocol: 1000 rpm for 10 s followed by 6000 rpm for 20 s. Chlorobenzene (200 μL) was dripped onto the spinning substrate 5 s before the end of the program. The substrates were then annealed for 1 h at 100 °C. The substrates were cooled to room temperature before deposition of the hole transporting material. A spiro-OMeTAD (Luminescence Technology) solution (70 mM in chlorobenzene) doped with bis(trifluoromethylsulfonyl)imide lithium salt (Li-TFSI), tris(2-(1*H*-pyrazol-1-yl)-4-*tert*-butylpyridine)−cobalt(III)tris(bis-(trifluorouoromethylsulfonyl)imide) (FK209, Dyenamo) and 4-*tert*-butylpyridine (TBP) was spun at 4000 rpm for 20 s. The molar ratios of additives for spiro-OMeTAD were 0.5, 0.03, and 3.3 for Li-TFSI, FK209, and TBP, respectively.

Scanning Electron Microscopy. A LEO 1550 FESEM (Zeiss) with a field emission source operated at an acceleration voltage of 2 kV was used.

Macroscopic Light $J-V$ Measurements. A solar simulator from ABET Technologies (Model 11016 Sun 2000) with a xenon arc lamp was used and the $J-V$ response was recorded using a Keithley 2635 source meter. The light source intensity was calibrated using a silicon reference cell from Czibula & Grundmann (FHG-ISE, RS-OD4). A scan rate of 50 mV/s was used for both reverse and forward scanning. All $J-V$ measurements were acquired in ambient conditions, 10 days after the devices were fabricated.

KPFM Measurements. The voltage measurements were performed using an Asylum Cypher S with blueDrive AFM at room temperature (~25 °C) in air that contained <10% relative humidity. We purposely kept the temperature and moisture level constant during the entirety of our experiments to avoid having convoluted contributions. The perovskite films were grounded using the FTO

DOI: 10.1021/acs.chemmater.9b03089
Chem. Mater. 2019, 31, 8969−8976

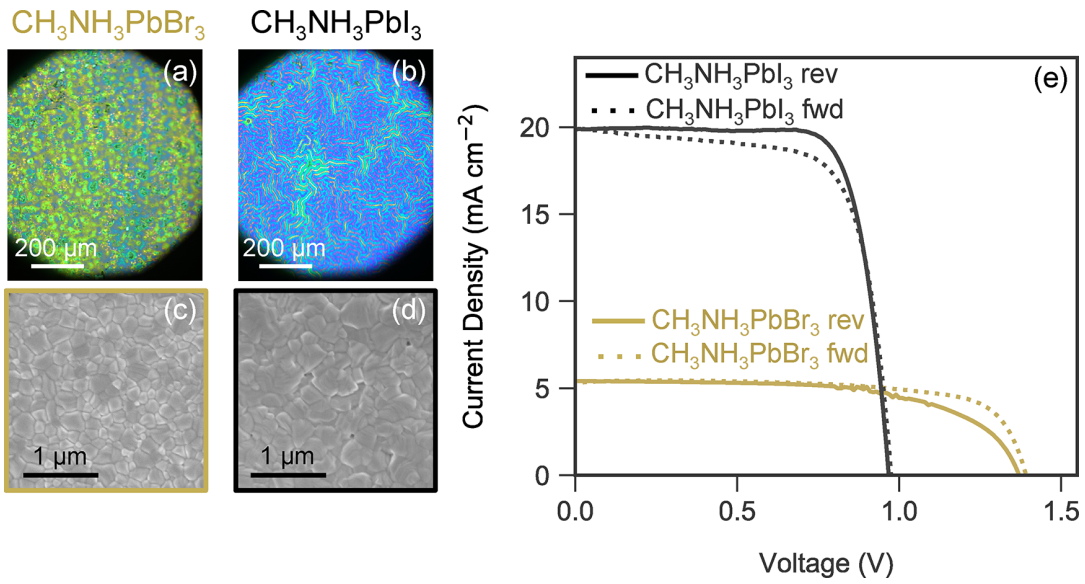

Figure 1. Optical and scanning electron microscopy images of (a,c) $CH_3NH_3PbBr_3$, and (b,d) $CH_3NH_3PbI_3$ perovskites. (e) Forward (dotted lines, fwd) and reverse (solid lines, rev) light $J-V$ curves for all perovskite full devices measured under AM1.5G illumination. Figures of merit for **forward** scans: $CH_3NH_3PbBr_3$: V_{oc} = 1.40 V, J_{sc} = 5.30 mA/cm^2, FF = 71.92%, η = 5.34%, $CH_3NH_3PbI_3$: V_{oc} = 0.98 V, J_{sc} = 19.99 mA/cm^2, FF = 70.38%, η = 13.78%, and **reverse** scans: $CH_3NH_3PbBr_3$: V_{oc} = 1.38 V, J_{sc} = 5.41 mA/cm^2, FF = 62.96%, η = 4.70%, $CH_3NH_3PbI_3$: V_{oc} = 0.97 V, J_{sc} = 19.86 mA/cm^2, FF = 77.16%, η = 14.86%.

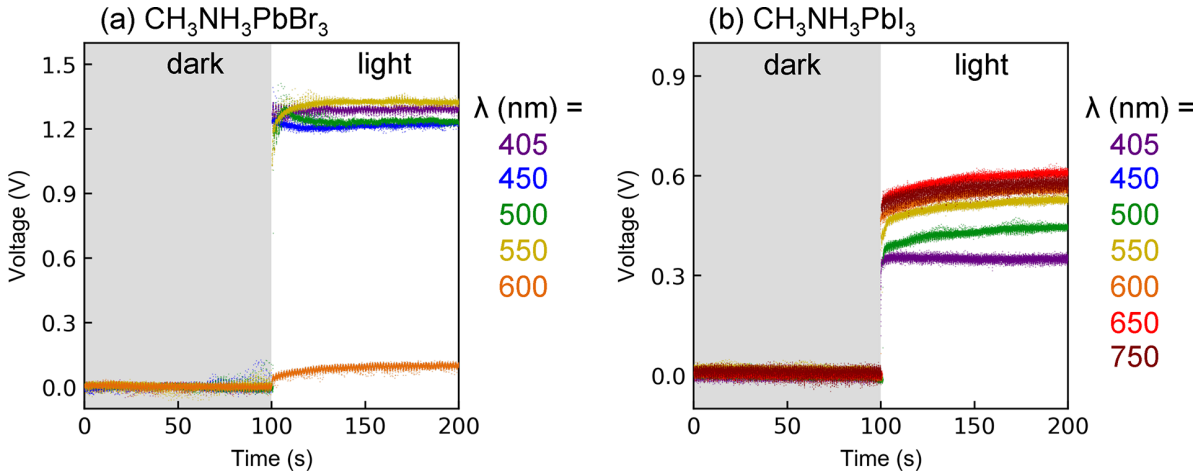

Figure 2. Voltage as a function of time for (a) $CH_3NH_3PbBr_3$ and (b) $CH_3NH_3PbI_3$ perovskites under dark (gray) and illuminated (white) conditions. For each wavelength the incident photon flux = 1 sun. The line color is matched to the photon energy used during the illumination treatment, indicated on the right side of each graph.

electrode while a Pt-coated Si AFM tip probed the top surface of the 200 nm Spiro-OMeTAD hole transport layer. The 405 nm illumination source was a single diode laser, while λ = 450−800 nm were filtered out from a broadband continuous laser (Fianium). The photon flux for each wavelength was equivalent to 1 sun, or 4.21 × 10^{21} photons/m^2/s, and the sequence of λ was chosen at random, thus mitigating the likelihood of any photon-energy-dependent trend in the relaxation times. The scan parameters for the $CH_3NH_3PbBr_3$ sample = 0.7 Hz, 256 × 256 pixels, and thus a time resolution of 2.79 ms/pixel. The parameters for $CH_3NH_3PbI_3$ perovskite = 1 Hz, 512 × 512 pixels, yielding a time resolution of 0.977 ms/pixel. Here we include both the trace and retrace KPFM data points for our time calculation. The voltage error (±20 mV) was determined by calculating the standard deviation of line scans on the KPFM maps.

Data Analysis. The KPFM trace and retrace images were combined and then flattened into time series vectors using standard linear algebra routines implemented in Python's Numpy library. The vector was then downsampled, using every fourth data point for 256 × 256 pixels maps and every eighth data point for 512 × 512 pixels images. The relaxation time is given by the median time of the data points contained within the first ∼5 s after the light is turned OFF with an average less than or equal to 10%, found using a sliding window approach with a step size of ∼1 s.

RESULTS AND DISCUSSION

Figure 1 displays optical and scanning electron microscopy (SEM) images for each perovskite sample, revealing the morphologies at different length scales. The optical micrographs captured with the atomic force microscopy (AFM) camera in Figure 1a,b present the unique μm- to mm-scale isotropic morphologies of each perovskite. The wrinkling exhibited by the $CH_3NH_3PbI_3$ film is a common feature of solution processing and may rise because of surface tension

DOI: 10.1021/acs.chemmater.9b03089
Chem. Mater. 2019, 31, 8969−8976

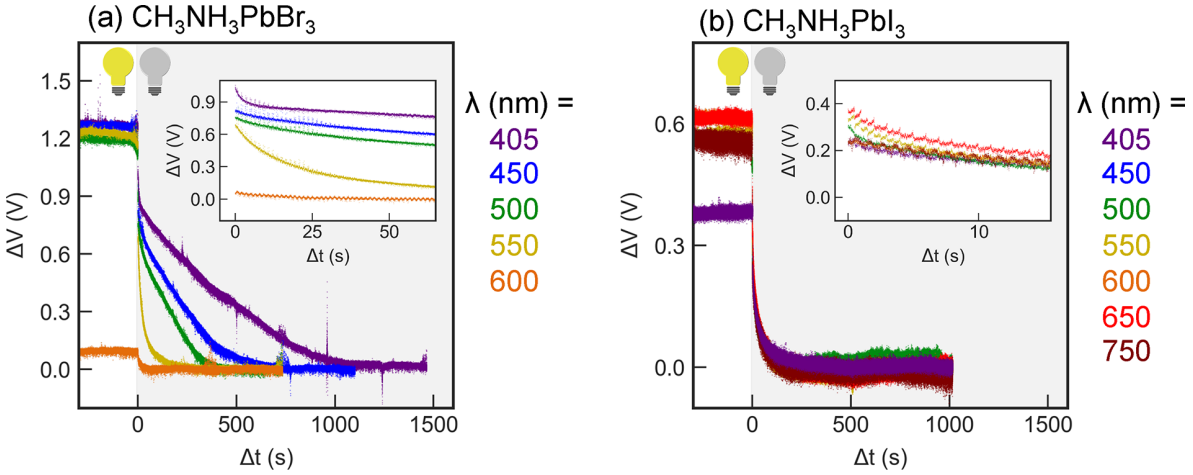

Figure 3. Postillumination (under dark conditions) voltage measurements ($\Delta V = V(t) - V_{final}$) as a function of time and wavelength for (a) $CH_3NH_3PbBr_3$ and (b) $CH_3NH_3PbI_3$ perovskites. The inset of each plot is a zoom in of the initial seconds of the voltage drop. The line color of each data set is matched to the λ of the illumination treatment.

during drying (Marangoni forces) or spinodal decomposition.[37] The SEM images (acquired on fresh thin films) in Figure 1c,d show the 100−500 nm grains with similar morphology. We fabricate photovoltaic devices with both perovskites (see light $J-V$ curves in Figure 1e for the performance of both compositions exhibiting minimal hysteresis).

We elucidate the influence of incident photon energy on the voltage dynamics of perovskites by conducting λ-dependent illuminated-KPFM experiments.[11,38] For all measurements, the light is incident on the TiO_2/FTO/glass side, with the probe scanning the top Spiro-OMeTAD hole transport layer. In all cases, the relative humidity is kept <10% (see the Experimental Section for more details and Figure S1 for a schematic of the experimental setup). When the perovskite films are initially illuminated, Figure 2, the photovoltage response is immediate (i.e., near the temporal resolution of the technique). Here, we show only the first 100 s before and after the light is switched ON to highlight the change in voltage response. The fast rise in photovoltage is dominated by electron−hole pair generation, or electronic motion, which occurs on the order of nanoseconds.[39] As expected, we measure no evident transient photon-energy dependent voltage behavior for any of the perovskites upon illumination. Yet, for the $CH_3NH_3PbI_3$ film (Figure 2b), the magnitude of the photovoltage varies as a function of λ. This is likely due to its variable quantum efficiency from the unoptimized layers as well as the presence of small amounts of PbI_2, which easily forms throughout the $CH_3NH_3PbI_3$ film and limits electrical performance of $\lambda < 520$ nm.[22,40] The laser is kept ON while monitoring the stabilization of the photovoltage response (note, the samples are illuminated for at least 8 min for any single wavelength). Importantly, there is no relationship found between the illumination time and subsequent voltage decay (see Table S1 for the order in which the measurements were acquired).

Once the illumination source is turned OFF, each perovskite solar cell displays unique voltage dynamics, as shown in Figure 3. The $CH_3NH_3PbBr_3$ perovskite (Figure 3a) has a strong λ-dependent voltage relaxation, where, consistent with previous macroscopic results,[21] the higher energy photons induce a slower voltage drop following the end of charge carrier generation which takes place on the order of nanoseconds. Note, the photon flux is equal for each incident wavelength and the films were kept in the dark until the final voltage value equilibrates within the error of the KPFM measurement of ±20 mV. The order of illuminated-KPFM measurements for the $CH_3NH_3PbBr_3$ sample is 550, 500, 450, 600, and 405 nm. Thus, after examining Figure 3a, it is clear that the voltage decay rates are independent of illumination history. To easily quantify the voltage changes during relaxation, we introduce the voltage term, ΔV, which is defined as $V(t) - V_{final}$ where $V(t)$ is the voltage response as a function of time and V_{final} is the last KPFM data point in the voltage time series curve in Figure 3. The voltage dynamics for the $CH_3NH_3PbI_3$ perovskite film are shown in Figure 3b. The relaxation behavior is unrelated to the incident photon excitation energy, at least within the temporal resolution of this experiment. Remarkably, the voltage drop for the perovskite samples is significantly slower ($>10^4$) in comparison to the dynamics presented in Figure 2, that is, the photovoltage rise time. The asymmetric voltage response[41] indicates that there are different electronic processes occurring before and after illumination. As previously described, we attribute the fast photovoltage rise time primarily to electron−hole pair generation and corresponding voltage production. The slower transient voltages after illumination are a combination of the end of electron−hole pair production and the relaxation of ion/defect motion initiated during illumination. The $CH_3NH_3PbI_3$ perovskite film equilibrates both faster and without a λ dependency compared with its $CH_3NH_3PbBr_3$ counterpart. Thus, in the $CH_3NH_3PbI_3$ perovskite, there are indeed ions/defects migrating; however, they move faster at shorter λ than the ions/defects in the $CH_3NH_3PbBr_3$ sample because of the less confined lattice structure, where the Pb−Br b-axis bond length = 3.031 Å, and the Pb−I b-axis bond length = 3.249 Å.[24] The binding energy (D) between the halides and Pb is inversely proportional to these bond lengths, with values of 201 and 142 kJ/mol, respectively. Based on the activation energies found in the literature for each ionic/defect species in these two perovskite compositions (see Table S2),[25,42−45] we argue that *all* ions and defects are contributing to the voltage decay rate, which we discuss in detail later. Perovskite topography maps before and after the illumination treatment are shown in the Supporting Information, Figure S2, where no changes in the morphology

DOI: 10.1021/acs.chemmater.9b03089
Chem. Mater. 2019, 31, 8969−8976

are observed during the KPFM measurements. The dark KPFM images present the spatially uniform voltage response that remains unchanged across multiple illumination cycles.

To quantify the voltage declination rate as a function of photon energy after the illumination source is switched OFF, we calculate the time required for the signal to decay to one-tenth of its initial residual voltage value for each wavelength-dependent measurement, plotted in Figure 4. Here, we use the 10% decay time because of its applicability to all wavelength-dependent measurements for both perovskite compositions, regardless of the combination of linear and exponential behavior present in the transient residual voltage. From Figure 3a and Figure 4, we observe relaxation times up to 829.95 s, for the $CH_3NH_3PbBr_3$ during the high-energy photoexcitation (405−500 nm, or 2.48−3.06 eV). In contrast, when exciting the charge carriers with lower energy photon levels, corresponding to incident λ = 550 nm (2.25 eV) and 600 nm (2.07 eV), the $CH_3NH_3PbBr_3$ relaxation times become similar to the $CH_3NH_3PbI_3$, indicating that similar relaxation processes are dominating the two halide perovskite samples within this excitation regime. Because 600 nm corresponds to photons with energy beyond the bandgap of $CH_3NH_3PbBr_3$, the time scale at this excitation wavelength is primarily associated with the relaxation of shallow trap states. The relaxation times for each λ and perovskite sample are given in the Supporting Information Table S3 and marked in Figures S3 and S4.

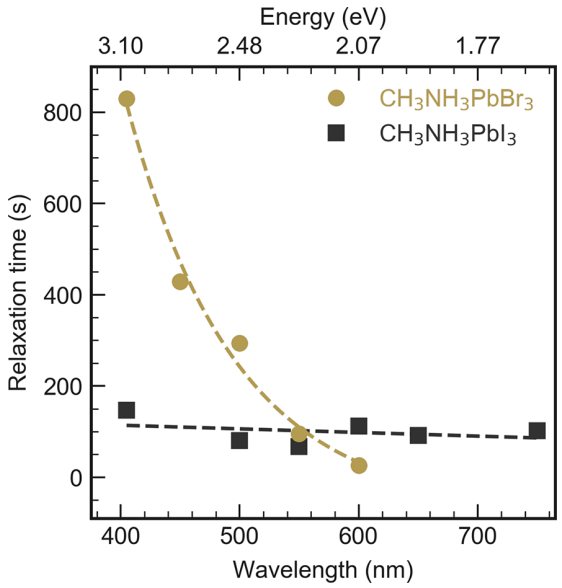

Figure 4. Relaxation time as a function of wavelength for postillumination voltage measurements in $CH_3NH_3PbBr_3$ (yellow circles) and $CH_3NH_3PbI_3$ (gray squares) perovskites. The dashed lines are best fits, and the slope for the $CH_3NH_3PbI_3$ fit is approximately zero (−0.08 s/nm).

Below we describe how the voltage relaxation times for the perovskites are due to a combination of factors unique to the specific material's composition. Throughout the duration of the illumination treatment, although the photovoltage value is stable in all cases (Figure 2), there are still many photoinduced mobile processes, both electronic and ionic, occurring.[34,46−50] Importantly, any halide phase segregation is unfeasible for the perovskites investigated here (two pure-halide perovskites); however, ion migration is still prevalent.[48] Additional transport mechanisms such as (i) electron−hole pair generation and separation, (ii) phonon-assisted ion motion,[49] (iii) charge carrier migration caused by filling of forbidden electronic states,[34] and (iv) heterogeneous strain within the perovskite lattice;[50] all coexist.

Figure 5 compiles the primary physical mechanisms that occur before, during, and after illumination, including the

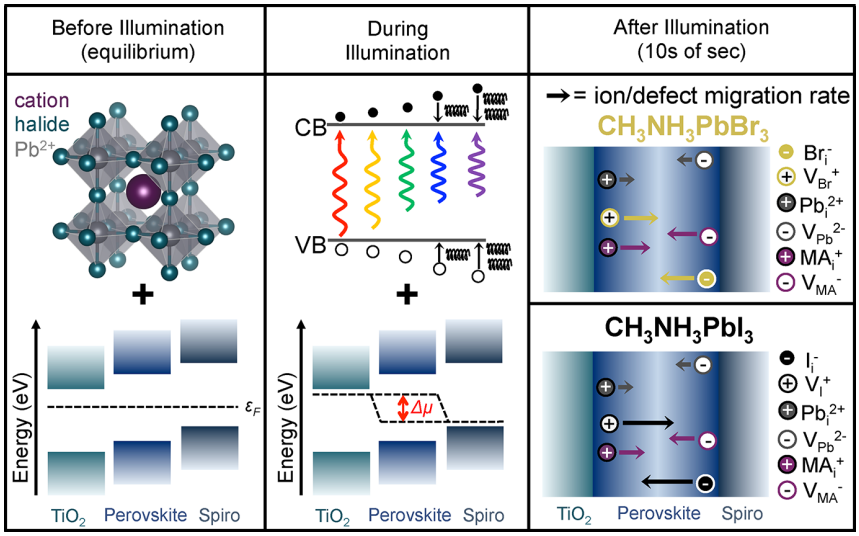

Figure 5. Illustration of the dynamic voltage behavior of the different perovskite compositions, before, during, and after illumination. All materials begin at equilibrium and during illumination generate charge carriers (i.e., quasi-Fermi level splitting ($\Delta\mu$)) and excess phonons dependent upon the incident photon energy. Seconds after the illumination is OFF, each perovskite undergoes individual voltage relaxation processes with their ion and defect migration qualitatively represented by the size of the color-coded arrow. Here, mobile ions within $CH_3NH_3PbI_3$ are not as constrained when compared with $CH_3NH_3PbBr_3$ while migrating back to the bulk of the perovskite. The graphics describe the electronic and ionic mechanisms relevant to explain the composition-dependent observed phenomena. White filled ions outlined in color = vacancies and ions filled with color = interstitials. Note: ion/defect migration direction and motion is not to scale for clarity.

DOI: 10.1021/acs.chemmater.9b03089
Chem. Mater. 2019, 31, 8969−8976

effects of photon excitation energies on the overall voltage response of the perovskites investigated here. Before illumination, the samples are in equilibrium, with atoms stable in the lattice positions and balanced energy states throughout the active layers of the devices. During illumination, charge carrier generation commences and there is quasi-Fermi level splitting ($\Delta\mu$), as expected. Here, we hypothesize that when higher energy photons are illuminating the perovskite surface, they generate excess phonons into the lattice (regardless of perovskite composition) because of the thermalization of the excited charge carriers (center of Figure 5). These phonons subsequently provoke extra ionic defects;[21] thus, once the illumination source is turned OFF, the quantity of mobile ions returning to equilibrium is larger. That is, the rate of ionic migration before returning to dark conditions correlates with the amount of energy lost to thermalization. Also, the illumination conditions used here (ranging from 400 to 600 nm (3.06−2.07 eV)) provide enough energy to activate the mobility of *all* atoms and defects in the $CH_3NH_3PbBr_3$ perovskite lattice,[46] with Pb^{2+} (E_A = 2.3 eV)[51] able to migrate the most at incident λ = 405, 450, and 500 nm, consistent with our experimental findings in Figures 3 and 4. We note that the literature provides a wide range of potential E_A values for Pb, as well as all other ionic defects, and here we are basing our discussion on the average cited values. For example, the I halide vacancy and interstitial E_A values average to be 0.28 and 0.195 eV,[24,25,42,44,45,51] respectively, and the Br halide vacancy and interstitials are 0.51 and 0.54 eV,[24,25,43] respectively. See Table S2 in Supporting Information for a collection of activation energies values from the literature. After illumination, the mobile ions and charged defects relax, and the rate of relaxation is perovskite-material dependent. The residual voltage response measured is a result of the charged mobile species moving back to their equilibrium positions, restored by the chemical potential generated by the previously photo-induced concentration gradient of ions/defects.[11] We propose that the $CH_3NH_3PbBr_3$ sample also shows a large wavelength dependency after illumination because of the smaller diameter of the Br^- halide atoms compared with that of I^-, which reduces the Pb−Br bond length and constricts the perovskite lattice structure. This restriction will abate ions from migrating throughout the crystal.[24] In the $CH_3NH_3PbI_3$ perovskite lattice, ion migration is prevalent, as its wavelength-independent relaxation time of ≈100 s (Figure 4) is in agreement with ion/defect relaxation time scales observed in similar structures.[21,39,41] However, not all prior studies measuring the transient voltage response quantify the decay time, and the methods for fitting the voltage relaxation time have yet to be unified. Additionally, there are likely residual PbI_2 clusters within the $CH_3NH_3PbI_3$ film which are utilizing some of the would-be mobile halide ions, shortening the observed photovoltage relaxation times. The possibility of depth-dependent photon absorption and, consequently, charge injection[52] within the perovskite material influencing these measurements is discounted, as the charge transport layers for both samples, are equivalent and the shortest excitation wavelengths, (i.e., shallowest absorption depths), demonstrate the largest voltage relaxation for $CH_3NH_3PbBr_3$. Further, our measurements are performed without the application of an external electric field, leaving ion migration as the main cause of the photovoltage dynamics. The influence of charge injection has been previously shown to lead to the formation of new defect centers that increase nonradiative recombination, but only in the presence of a 0.9 V/μm field.[53] We also exclude charge carrier recombination as a primary source for the slow voltage decay, as prior studies performing time-dependent photoluminescence measurements as a function of excitation wavelength found that ion migration explains the differences in the rate of hole transfer[54] and photodegradation.[55]

CONCLUSIONS

In summary, we captured the transient voltage of photovoltaic halide perovskites as a function of incident photon energy (2.0−1.65 eV). Upon initial light exposure, both $CH_3NH_3PbBr_3$ and $CH_3NH_3PbI_3$ displayed fast photovoltage responses, regardless of λ. However, when the illumination source was switched OFF, we discovered a > 10^4 slower voltage decline for both solar cell materials. Remarkably, the $CH_3NH_3PbBr_3$ sample exhibited a stark photon energy-dependent electrical behavior, with voltage relaxation times up to 10× larger than $CH_3NH_3PbI_3$. The slower λ-dependent dynamics observed in the Br perovskite are due to (i) Br's smaller atomic radius which indicates stronger bonding between the Pb^{2+} and Br^-, hindering ion motion due to the constrained lattice, (ii) an excess number of phonons caused by higher energy photons thermalizing down to the conduction band; and (iii) excitation energies beyond the E_A of Pb, introducing an extra mobile ion into the lattice. Meanwhile, the electrical response of the other perovskite composition, $CH_3NH_3PbI_3$, demonstrated consistent voltage relaxation times regardless of incident wavelength, with an average duration of 100 s. We hypothesize that this faster relaxation is primarily due to the lower Pb−I binding energy. The transient voltage measurements presented here revealed an unforeseen variable, incident photon energy, which is fundamentally linked to the time scales of perovskite's optoelectronic properties.

Our results call for new ways to rationally design perovskites with controlled electrical response, either by eradicating the λ-dependency or by leveraging it for optoelectronics. We foresee the development of next-generation photodetector devices used to discern between different photon energies based on the response time to the incident light, enabling new, inexpensive spectral detection sensors. Future experiments will evaluate the time-dependent voltage as a function of λ-dependent *and* operating parameters (O_2, H_2O, and temperature) to further elucidate the chemical processes governing electrical dynamics in metal halide perovskites. For these experiments, we anticipate that machine learning approaches will play a critical role in predicting perovskites' photoresponse given the vast combinatorial space of these environmental stressors, and the higher number of perovskite chemical compositions.[1]

ASSOCIATED CONTENT

Supporting Information

The Supporting Information is available free of charge on the ACS Publications website at DOI: 10.1021/acs.chemmater.9b03089.

KPFM experimental setup, table of order of measurements, before and after AFM topography images, dark KPFM images, table of activation energies from literature, table of voltage relaxation times, postillumination KPFM voltage decays (PDF)

DOI: 10.1021/acs.chemmater.9b03089
Chem. Mater. 2019, 31, 8969−8976

AUTHOR INFORMATION

Corresponding Author

*E-mail: mleite@umd.edu.

ORCID

Elizabeth M. Tennyson: 0000-0003-0071-8445
John M. Howard: 0000-0002-3990-5478
Joseph L. Garrett: 0000-0001-8265-0661
Jeremy N. Munday: 0000-0002-0881-9876
Marina S. Leite: 0000-0003-4888-8195

Author Contributions

[∇]E.M.T. and J.M.H. contributed equally. M.S.L. conceived the research project. E.M.T. performed the KPFM measurements, B.R. fabricated the perovskite samples, and J.L.G. developed the fast KPFM method. E.M.T., J.M.H., and M.S.L. analyzed the data and wrote the manuscript. All authors discussed the results and contributed to the text. All authors have given approval to the final version of the manuscript. .

Notes

The authors declare no competing financial interest.

ACKNOWLEDGMENTS

The authors thank the financial support from NSF (ECCS, award 16-10833), APS Ovshinsky Sustainable Energy Fellowship, the UMD All-S.T.A.R. Fellowship, the 2017-2018 UMD Hulka Energy Research Fellowship, the 2018-2019 UMD Harry K. Wells Graduate Fellowship, and the UMD Department of Physics through The Thomas Mason Interdisciplinary Physics Fund.

REFERENCES

(1) Howard, J. M.; Tennyson, E. M.; Neves, B. R. A.; Leite, M. S. Machine Learning for Perovskites' Reap-Rest-Recovery Cycle. *Joule* **2019**, *3*, 325−337.

(2) Green, M. A.; Ho-Baillie, A. Perovskite Solar Cells: The Birth of a New Era in Photovoltaics. *ACS Energy Lett.* **2017**, *2*, 822−830.

(3) Roose, B.; Wang, Q.; Abate, A. The Role of Charge Selective Contacts in Perovskite Solar Cell Stability. *Adv. Energy Mater.* **2018**, 1803140.

(4) Rosales, B. A.; Hanrahan, M. P.; Boote, B. W.; Rossini, A. J.; Smith, E. A.; Vela, J. Lead Halide Perovskites: Challenges and Opportunities in Advanced Synthesis and Spectroscopy. *ACS Energy Lett.* **2017**, *2*, 906−914.

(5) Zong, Y.; Zhou, Y.; Zhang, Y.; Li, Z.; Zhang, L.; Ju, M.-G.; Chen, M.; Pang, S.; Zeng, X. C.; Padture, N. P. Continuous Grain-Boundary Functionalization for High-Efficiency Perovskite Solar Cells with Exceptional Stability. *Chem.* **2018**, *4*, 1404−1415.

(6) Noel, N. K.; Wenger, B.; Habisreutinger, S. N.; Patel, J. B.; Crothers, T.; Wang, Z.; Nicholas, R. J.; Johnston, M. B.; Herz, L. M.; Snaith, H. J. Highly Crystalline Methylammonium Lead Tribromide Perovskite Films for Efficient Photovoltaic Devices. *ACS Energy Lett.* **2018**, *3*, 1233−1240.

(7) Stoddard, R. J.; Eickemeyer, F. T.; Katahara, J. K.; Hillhouse, H. W. Correlation between Photoluminescence and Carrier Transport and a Simple In Situ Passivation Method for High-Bandgap Hybrid Perovskites. *J. Phys. Chem. Lett.* **2017**, *8*, 3289−3298.

(8) Sutter-Fella, C. M.; Li, Y.; Amani, M.; Ager, J. W.; Toma, F. M.; Yablonovitch, E.; Sharp, I. D.; Javey, A. High Photoluminescence Quantum Yield in Band Gap Tunable Bromide Containing Mixed Halide Perovskites. *Nano Lett.* **2016**, *16*, 800−806.

(9) Slotcavage, D. J.; Karunadasa, H. I.; McGehee, M. D. Light-Induced Phase Segregation in Halide-Perovskite Absorbers. *ACS Energy Lett.* **2016**, *1*, 1199−1205.

(10) Phung, N.; Abate, A. The Impact of Nano- and Microstructure on the Stability of Perovskite Solar Cells. *Small* **2018**, *14*, e1802573.

(11) Garrett, J. L.; Tennyson, E. M.; Hu, M.; Huang, J.; Munday, J. N.; Leite, M. S. Real-Time Nanoscale Open-Circuit Voltage Dynamics of Perovskite Solar Cells. *Nano Lett.* **2017**, *17*, 2554−2560.

(12) Howard, J. M.; Tennyson, E. M.; Barik, S.; Szostak, R.; Waks, E.; Toney, M. F.; Nogueira, A. F.; Neves, B. R. A.; Leite, M. S. Humidity-Induced Photoluminescence Hysteresis in Variable Cs/Br Ratio Hybrid Perovskites. *J. Phys. Chem. Lett.* **2018**, *9*, 3463−3469.

(13) Huang, J.; Tan, S.; Lund, P. D.; Zhou, H. Impact of H_2O on Organic-Inorganic Hybrid Perovskite Solar Cells. *Energy Environ. Sci.* **2017**, *10*, 2284−2311.

(14) Tian, Y.; Peter, M.; Unger, E.; Abdellah, M.; Zheng, K.; Pullerits, T.; Yartsev, A.; Sundström, V.; Scheblykin, I. G. Mechanistic Insights into Perovskite Photoluminescence Enhancement: Light Curing with Oxygen can Boost Yield Thousandfold. *Phys. Chem. Chem. Phys.* **2015**, *17*, 24978−24987.

(15) Motti, S. G.; Gandini, M.; Barker, A. J.; Ball, J. M.; Kandada, A. R. S.; Petrozza, A. Photoinduced Emissive Trap States in Lead Halide Perovskite Semiconductors. *ACS Energy Lett.* **2016**, *1*, 726−730.

(16) Cao, R.; Xu, F.; Zhu, J.; Ge, S.; Wang, W.; Xu, H.; Xu, R.; Wu, Y.; Ma, Z.; Hong, F.; Jiang, Z. Unveiling the Low-Temperature Pseudodegradation of Photovoltaic Performance in Planar Perovskite Solar Cell by Optoelectronic Observation. *Adv. Energy Mater.* **2016**, *6*, 1600814.

(17) Duong, T.; Wu, Y.; Shen, H.; Peng, J.; Zhao, S.; Wu, N.; Lockrey, M.; White, T.; Weber, K.; Catchpole, K. Light and Elevated Temperature Induced Degradation (LeTID) in Perovskite Solar Cells and Development of Stable Semi-Transparent Cells. *Sol. Energy Mater. Sol. Cells* **2018**, *188*, 27−36.

(18) Barbé, J.; Kumar, V.; Newman, M. J.; Lee, H. K. H.; Jain, S. M.; Chen, H.; Charbonneau, C.; Rodenburg, C.; Tsoi, W. C. Dark Electrical Bias Effects on Moisture-Induced Degradation in Inverted Lead Halide Perovskite Solar Cells Measured by Using Advanced Chemical Probes. *Sustainable Energy Fuels* **2018**, *2*, 905−914.

(19) Hentz, O.; Rekemeyer, P.; Gradečak, S. Effects of Voltage Biasing on Current Extraction in Perovskite Solar Cells. *Adv. Energy Mater.* **2018**, *8*, 1701378.

(20) Grancini, G.; Roldán-Carmona, C.; Zimmermann, I.; Mosconi, E.; Lee, X.; Martineau, D.; Narbey, S.; Oswald, F.; De Angelis, F.; Graetzel, M.; Nazeeruddin, M. K. One-Year Stable Perovskite Solar Cells by 2D/3D Interface Engineering. *Nat. Commun.* **2017**, *8*, 15684.

(21) Pazoki, M.; Jacobsson, T. J.; Cruz, S. H. T.; Johansson, M. B.; Imani, R.; Kullgren, J.; Hagfeldt, A.; Johansson, E. M. J.; Edvinsson, T.; Boschloo, G. Photon Energy-Dependent Hysteresis Effects in Lead Halide Perovskite Materials. *J. Phys. Chem. C* **2017**, *121*, 26180−26187.

(22) Quitsch, W.-A.; deQuilettes, D. W.; Pfingsten, O.; Schmitz, A.; Ognjanovic, S.; Jariwala, S.; Koch, S.; Winterer, M.; Ginger, D. S.; Bacher, G. The Role of Excitation Energy in Photobrightening and Photodegradation of Halide Perovskite Thin Films. *J. Phys. Chem. Lett.* **2018**, *9*, 2062−2069.

(23) Juarez-Perez, E. J.; Ono, L. K.; Maeda, M.; Jiang, Y.; Hawash, Z.; Qi, Y. Photodecomposition and Thermal Decomposition in Methylammonium Halide Lead Perovskites and Inferred Design Principles to Increase Photovoltaic Device Stability. *J. Mater. Chem. A* **2018**, *6*, 9604−9612.

(24) Lin, C.; Li, S.; Zhang, W.; Shao, C.; Yang, Z. Effect of Bromine Substitution on the Ion Migration and Optical Absorption in $MAPbI_3$ Perovskite Solar Cells: The First-Principles Study. *ACS Appl. Energy Mater.* **2018**, *1*, 1374−1380.

(25) Azpiroz, J. M.; Mosconi, E.; Bisquert, J.; De Angelis, F. Defect Migration in Methylammonium Lead Iodide and its Role in Perovskite Solar Cell Operation. *Energy Environ. Sci.* **2015**, *8*, 2118−2127.

(26) Tennyson, E. M.; Garrett, J. L.; Frantz, J. A.; Myers, J. D.; Bekele, R. Y.; Sanghera, J. S.; Munday, J. N.; Leite, M. S. Nanoimaging of Open-Circuit Voltage in Photovoltaic Devices. *Adv. Energy Mater.* **2015**, *5*, 1501142.

(27) Tennyson, E. M.; Roose, B.; Garrett, J. L.; Gong, C.; Munday, J. N.; Abate, A.; Leite, M. S. Cesium-Incorporated Triple Cation

DOI: 10.1021/acs.chemmater.9b03089
Chem. Mater. 2019, 31, 8969−8976

Perovskites Deliver Fully Reversible and Stable Nanoscale Voltage Response. *ACS Nano* **2019**, *13*, 1538−1546.
(28) Tennyson, E. M.; Howard, J. M.; Leite, M. S. Mesoscale functional imaging of materials for photovoltaics. *ACS Energy Lett.* **2017**, *2*, 1825−1834.
(29) Garrett, J. L.; Munday, J. N. Fast, High-Resolution Surface Potential Measurements in Air with Heterodyne Kelvin Probe Force Microscopy. *Nanotechnology* **2016**, *27*, 245705.
(30) Collins, L.; Ahmadi, M.; Wu, T.; Hu, B.; Kalinin, S. V.; Jesse, S. Breaking the Time Barrier in Kelvin Probe Force Microscopy: Fast Free Force Reconstruction Using the G-Mode Platform. *ACS Nano* **2017**, *11*, 8717−8729.
(31) Guo, Z.; Wan, Y.; Yang, M.; Snaider, J.; Zhu, K.; Huang, L. Long-Range Hot-Carrier Transport in Hybrid Perovskites Visualized by Ultrafast Microscopy. *Science* **2017**, *356*, 59−62.
(32) Yoon, S. J.; Draguta, S.; Manser, J. S.; Sharia, O.; Schneider, W. F.; Kuno, M.; Kamat, P. V. Tracking Iodide and Bromide Ion Segregation in Mixed Halide Lead Perovskites during Photoirradiation. *ACS Energy Lett.* **2016**, *1*, 290−296.
(33) Yoon, S. J.; Kuno, M.; Kamat, P. V. Shift Happens. How Halide Ion Defects Influence Photoinduced Segregation in Mixed Halide Perovskites. *ACS Energy Lett.* **2017**, *2*, 1507−1514.
(34) Hoke, E. T.; Slotcavage, D. J.; Dohner, E. R.; Bowring, A. R.; Karunadasa, H. I.; McGehee, M. D. Reversible Photo-Induced Trap Formation in Mixed-Halide Hybrid Perovskites for Photovoltaics. *Chem. Sci.* **2015**, *6*, 613−617.
(35) Tennyson, E. M.; Gong, C.; Leite, M. S. Imaging Energy Harvesting and Storage Systems at the Nanoscale. *ACS Energy Lett.* **2017**, *2*, 2761−2777.
(36) Tennyson, E. M.; Howard, J. M.; Leite, M. S. Mesoscale Functional Imaging of Materials for Photovoltaics. *ACS Energy Lett.* **2017**, *2*, 1825−1834.
(37) Bercegol, A.; Ramos, F. J.; Rebai, A.; Guillemot, T.; Puel, J.-B.; Guillemoles, J.-F.; Ory, D.; Rousset, J.; Lombez, L. Spatial Inhomogeneity Analysis of Cesium-Rich Wrinkles in Triple-Cation Perovskite. *J. Phys. Chem. C* **2018**, *122*, 23345−23351.
(38) Almadori, Y.; Moerman, D.; Martinez, J. L.; Leclère, P.; Grévin, B. Multimodal Noncontact Atomic Force Microscopy and Kelvin Probe Force Microscopy Investigations of Organolead Tribromide Perovskite Single Crystals. *Beilstein J. Nanotechnol.* **2018**, *9*, 1695−1704.
(39) Pockett, A.; Eperon, G. E.; Sakai, N.; Snaith, H. J.; Peter, L. M.; Cameron, P. J. Microseconds, Milliseconds and Seconds: Deconvoluting the Dynamic Behaviour of Planar Perovskite Solar Cells. *Phys. Chem. Chem. Phys.* **2017**, *19*, 5959−5970.
(40) Jacobsson, T. J.; Correa-Baena, J.-P.; Halvani Anaraki, E.; Philippe, B.; Stranks, S. D.; Bouduban, M. E. F.; Tress, W.; Schenk, K.; Teuscher, J.; Moser, J.-E.; Rensmo, H.; Hagfeldt, A. Unreacted PbI_2 as a Double-Edged Sword for Enhancing the Performance of Perovskite Solar Cells. *J. Am. Chem. Soc.* **2016**, *138*, 10331−10343.
(41) Hu, J. G.; Gottesman, R.; Gouda, L.; Kama, A.; Priel, M.; Tirosh, S.; Bisquert, J.; Zaban, A. Photovoltage Behavior in Perovskite Solar Cells under Light-Soaking Showing Photoinduced Interfacial Changes. *ACS Energy Lett.* **2017**, *2*, 950−956.
(42) Mosconi, E.; Meggiolaro, D.; Snaith, H. J.; Stranks, S. D.; De Angelis, F. Light-Induced Annihilation of Frenkel Defects in Organo-Lead Halide Perovskites. *Energy Environ. Sci.* **2016**, *9*, 3180−3187.
(43) Oranskaia, A.; Yin, J.; Bakr, O. M.; Brédas, J. L.; Mohammed, O. F. Halogen Migration in Hybrid Perovskites: The Organic Cation Matters. *J. Phys. Chem. Lett.* **2018**, *9*, 5474−5480.
(44) Delugas, P.; Caddeo, C.; Filippetti, A.; Mattoni, A. Thermally Activated Point Defect Diffusion in Methylammonium Lead Trihalide: Anisotropic and Ultrahigh Mobility of Iodine. *J. Phys. Chem. Lett.* **2016**, *7*, 2356−2361.
(45) Yang, D.; Ming, W.; Shi, H.; Zhang, L.; Du, M.-H. Fast Diffusion of Native Defects and Impurities in Perovskite Solar Cell Material $CH_3NH_3PbI_3$. *Chem. Mater.* **2016**, *28*, 4349−4357.
(46) Walsh, A.; Stranks, S. D. Taking Control of Ion Transport in Halide Perovskite Solar Cells. *ACS Energy Lett.* **2018**, *3*, 1983−1990.
(47) Lang, F.; Shargaieva, O.; Brus, V. V.; Rappich, J.; Nickel, N. H. Creation and Annealing of Metastable Defect States in $CH_3NH_3PbI_3$ at Low Temperatures. *Appl. Phys. Lett.* **2018**, *112*, 081102.
(48) Yuan, Y.; Huang, J. Ion Migration in Organometal Trihalide Perovskite and Its Impact on Photovoltaic Efficiency and Stability. *Acc. Chem. Res.* **2016**, *49*, 286−293.
(49) Barboni, D.; De Souza, R. A. The Thermodynamics and Kinetics of Iodine Vacancies in the Hybrid Perovskite Methylammonium Lead Iodide. *Energy Environ. Sci.* **2018**, *11*, 3266−3274.
(50) Bischak, C. G.; Hetherington, C. L.; Wu, H.; Aloni, S.; Ogletree, D. F.; Limmer, D. T.; Ginsberg, N. S. Origin of Reversible Photoinduced Phase Separation in Hybrid Perovskites. *Nano Lett.* **2017**, *17*, 1028−1033.
(51) Eames, C.; Frost, J. M.; Barnes, P. R. F.; O'Regan, B. C.; Walsh, A.; Islam, M. S. Ionic Transport in Hybrid Lead Iodide Perovskite Solar Cells. *Nat. Commun.* **2015**, *6*, 7497.
(52) Tennyson, E. M.; Frantz, J. A.; Howard, J. M.; Gunnarsson, W. B.; Myers, J. D.; Bekele, R. Y.; Sanghera, J. S.; Na, S.-M.; Leite, M. S. Photovoltage Tomography in Polycrystalline Solar Cells. *ACS Energy Lett.* **2016**, *1*, 899−905.
(53) Birkhold, S. T.; Precht, J. T.; Liu, H.; Giridharagopal, R.; Eperon, G. E.; Schmidt-Mende, L.; Li, X.; Ginger, D. S. Interplay of Mobile Ions and Injected Carriers Creates Recombination Centers in Metal Halide Perovskites under Bias. *ACS Energy Lett.* **2018**, *3*, 1279−1286.
(54) Zheng, F.; Wen, X.; Bu, T.; Chen, S.; Yang, J.; Chen, W.; Huang, F.; Cheng, Y.; Jia, B. Slow Response of Carrier Dynamics in Perovskite Interface upon Illumination. *ACS Appl. Mater. Interfaces* **2018**, *10*, 31452−31461.
(55) Motti, S. G.; Meggiolaro, D.; Barker, A. J.; Mosconi, E.; Perini, C. A. R.; Ball, J. M.; Gandini, M.; Kim, M.; De Angelis, F.; Petrozza, A. Controlling Competing Photochemical Reactions Stabilizes Perovskite Solar Cells. *Nat. Photonics* **2019**, *13*, 532−539.

DOI: 10.1021/acs.chemmater.9b03089
Chem. Mater. 2019, 31, 8969−8976